25th ABCM International Congress of Mechanical Engineering
October 20-25, 2019, Uberlândia, MG, Brazil

COB-2019-0714
EXPERIMENTAL MEASUREMENTS OF PRESSURE AND VELOCITY FIELDS AROUND CIRCULAR CYLINDERS ARRANGED IN PAIRS

José Leandro Cardoso Rivera Vila[1]
Pedro Paulo Silva de Almeida[2]
Thiago Ferreira Gomes[3]
Tiago de Melo[4]
Jhon Nero Vaz Goulart[5]
[1,2,4]Centro Universitário do Distrito Federal – UDF, Brasília, 70.390-045, Brasil
[3,5]Group of Experimental and Computational Mechanics, University of Brasilia, Gama, 72.405-610, Brazil
[1]jl.vila@hotmail.com, [2]almeidappsa@gmail.com, [3]fgomes.thiago@gmail.com,[4]tiago.melomec@gmail.com, [5]jvaz@unb.br

Abstract. *In this paper the pressure field and its fluctuation around circular cylinders arranged in pairs will be measured, as well as the wake characteristics behind each cylinder. The experimental investigation is carried out in an aerodynamic channel with turbulence intensity of free stream less than 3%. The pressure and its fluctuation were gathered through a pressure transducer whereas the velocity fields were measured by using single hot-wire probes. Mathematical tools were employed to identify flow patterns in the velocity and pressure time-traces. During the experimental campaign three p/d-ratio were tested, p/d = 1.26, 2.00 and 3.00, for a constant Reynolds number, $Re_D = 1.78 \times 10^4$, based on the circular cylinder diameter, D, the free stream velocity, U_∞, and the kinematic viscosity of the fluid, ν. Through the pressure measurements it was identified that the mean average pressure distribution around the cylinders departs from the that one takes place in a single cylinder as the p/d-ratio decreases. As regards the dynamic of the flow two distinguished behaviors were observed: for intermediated p/d-ratio (2 and 3), the Strouhal number was found slighted superior to 0.21, on the other hand, for the lowest p/d-ratio, the pressure spectrum did not present important peaks. Time-frequency tools were also employed to analyze the dynamic behavior of the flow velocity behind the circular cylinders showing a kind of intermittent process in the vortex shedding when the p/d-ratio decreases.*

Keywords: *Turbulent flow, Two cylinders side-by-side, Wake Interactions, Bistability, Subcritical regime.*

1. INTRODUCTION

Flow over a single circular cylinder is one simple structure submitted to cross flow in vast engineering scenarios. Cylinders arranged in pairs are widely used in transmission lines, heat exchangers, cores of nuclear reactors and steam generators. In order to raise awareness on the flow field around circular cylinders experimental campaign was carried out by Žukauskas (1972), followed by his later works Žukauskas et al. (1980) and Žukauskas and Katinas (1988). In these works the authors were very concerned to outline the basis for heat transfer prediction in bank tubes, for instance (Žukauskas, 1972). Nowadays works from Ahamad et al. (2018), Alam et al. (2017), Kim and Alam (2015), Sumner (2010), among others, are concerned with the wake interactions behind the cylinders when the gap between them changes. One of the most remarkable features of the flow around circular cylinders arranged in pairs (or even in banks) is the wake interactions. The interaction between wakes behind the cylinders depends much more on the proximity between the cylinders than the Reynolds number. Such interaction causes two types of wakes, producing stable topologies that randomly changes over time (Neumeister et al., 2018). This phenomenon is so called bistable flow.

Bistable flow leads to an asymmetric flow behind the cylinders, forming dissimilar wakes (NW – narrow wake and WW – wide wake). The aerodynamic forces on the cylinder's surfaces and the dynamic of the flow are ruled by the wake topology experienced by each cylinder (Alam et al., 2003, Kang, 2003, Wang and Zhou, 2005, Giacomello et al., 2006). Numerical and experimental works have been aimed to study the bistability process either in rows of cylinders or pair of them (Olinto et al., 2006, Olinto et al., 2009, de Paula et al., 2012, 2013 and 2018). Kang, 2003, carried out a numerical work for various Reynolds numbers and T/D-ratios (T = p/d – 1). From the numeric results the author identified up to six different wakes topologies, depending on the distance between the centers of the cylinders and the Reynolds number. The author also stated that, for the studied Reynolds range, the frequency of vortex detachment is influenced mainly by the spacing between the cylinders. For 0.5 < T/D <1.5 the vortex frequency drops, on the other hand the drag coefficients depend mainly on the spacing between the cylinders. Finally, for T/D-ratio higher than 3 the flow becomes significantly dependent on the Reynolds number only.

In this paper the velocity in the wakes and the pressure time-traces on the cylinder's surface are experimentally measured in a pair of circular cylinders under a subcritical Reynolds of $Re = 1.78 \times 10^4$. The Reynolds number and the cylinder's diameter were kept constant throughout the experimental campaign. Three different p/d-ratio were investigated, 1.26, 2.00 and 3.00. The mean pressure distribution, as a function of the angular position around the cylinder's surface, was found to depart from that one stressed in a single cylinder as the p/d-ratio decreases. The Strouhal number was also target of our investigation. The vortex shedding frequency was seen almost unchangeable for p/d = 2 and 3, very close to 0.21. On the other hand, when the cylinder was under the lowest p/d-ratio the spectral analyses did not present a significant peak.

2. EXPERIMENTAL ARRANGEMENT

Flow over the side-by-side cylinders was investigated in a 4000 (mm) long aerodynamic channel with a 150 x 200 (mm) transversal section. The air is driven by a centrifugal blower connected to a frequency inverter. Before reaching the circular cylinders the flow passes by several devices in order to reduce the free stream turbulence intensity, that is less than 3%. A Pitot Tube is placed 150 mm downstream from the channel's inlet to measure the reference velocity U_∞.

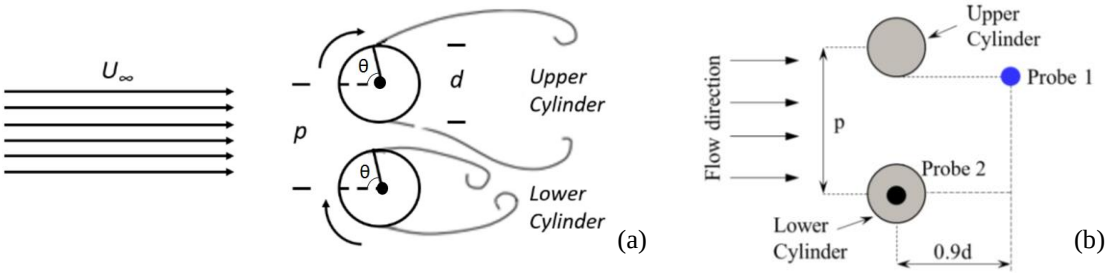

Figure 1. Schematic view of the flow reaching the cylinders. (a) pressure transducer moving position tap indication; (b) hot-wire probes positioning.

The pressure time-traces were acquired by using a piezoresistive pressure transducer Endevco 8510B-01 (Probe 2), connected to an ENDEVCO® Model 136 DC Amplifier. The dynamic pressure signals were gathered over the cylinder's surfaces at each 10°, from 0° up to 360° through 1 mm pressure tap. The pressure tap is the same showed by Goulart et al., 2003. The angular position 0° is taken when the position is facing the main flow. Figure 1 (a) shows the angular positions where pressure time-traces were gathered.

Wake interactions were also investigated by employing hot-wire anemometry technique. Velocity fields were measured downstream the cylinders with a DANTEC® 55P11 hot-wire probe (Probe 1), 0.9D far from the cylinders, see Fig. 1 (b). During the experiments both pressure (Probe 2) and velocity (Probe 1) data were sampled at 4.0 kHz. A low pass filter was set at 2 kHz. Time series were 32.768 s long. Data acquisition was performed using a 12 bit TSI A/D 8 CH converter board. As regards the uncertainness about the pressure and velocity data we estimated that the pressure spectrum possesses up to 6.0 % whilst the velocity data, by following the steps suggested by Moffat (1988) it was estimated to reach up to 10%, in terms of velocity.

3. RESULTS AND DISCUSSIONS

3.1 Mean Average Pressure Distribution

The pressure coefficient, *Cp*, distribution is disposed in Fig. 2 (a up to d), as a function of the angular position around the tubes. The mean average pressure coefficient is then computed through Eq. (1):

$$Cp = \frac{p - p_\infty}{\frac{1}{2}\rho U^2} \tag{1}$$

, where p is the static pressure at the point of measure, p_∞ is the free stream dynamic pressure, ρ is the density of the fluid, and U is the free stream velocity. In Fig. 2 (a) we show the mean pressure distribution for a single cylinder. From this figure we can see that our system acquisition works in good way and the measurements obtained for a single cylinder are in good agreement with the open literature. The mean average pressure distribution is very symmetric reaching the highest and lowest values of Cp at 0° and about 60°, respectively. As regards to the energy fluctuation of the pressure traces we also calculated the root mean square (RMS) of the signal. The RMS of the pressure fluctuation is depicted as angular position function. The RMS is calculated by Eq. (2) as:

$$Cpf = \sqrt{\frac{\overline{p_\theta^{'2}}}{\frac{1}{2}\rho U_\infty^2}} \tag{2}$$

Fig. 2 (b) stresses the RMS values of each position on the circular cylinder's surface. The most energetic positions are located at 80º and 280º degrees, emphasizing the points of boundary layer detachment. The energy peaks are roughly 0.26. Both peaks location and its values are in great agreement with the work conducted by Pang et al. (2016), whom conducted an experimental campaign to measure the mean average and fluctuant quantities of pressure around single circular cylinders. Once the pressure acquisition system had been set, producing satisfactory outcomes using a single circular cylinder as benchmark, we furthered our experimental campaign by measuring the mean average pressure in a pair of circular cylinders. Mean average *Cp* as an angular position function for 3 different p/d-ratios is shown in Fig. 2 (c) and (d), for the upper and lower cylinders, respectively.

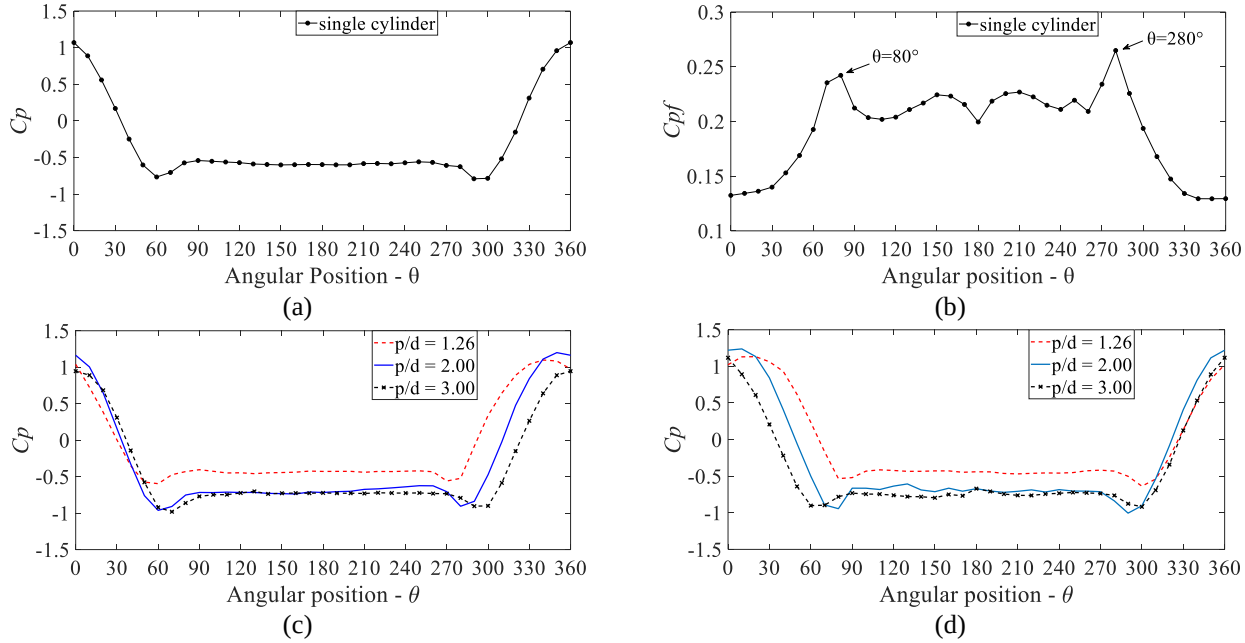

Figure 2. Pressure coefficient distribution on the cylinder's surface as a function of the angular position. (a) single circular cylinder; (b) fluctuating pressure coefficient for the single cylinder; (c) upper circular cylinder; (d) lower circular cylinder.

From the figures it is remarkable the pressure distribution divergence as the p/d-ratio decreases. Moreover, the stagnation point moves towards the tight gap as the distance between cylinders decreases. As regards the lowest pressure both cylinders presented the same value, at about Cp = -1.0, for p/d-ratios of 2.00 and 3.00. However, a distinguished behavior takes place for the lowest p/d-ratio. For such, the pressure around the cylinder increases, reaching Cp ~ -0.50. These results are in agreement with the studies of Pang et al. (2016) and Afgan et al. (2011).

3.2 Wake interactions

As said before a single hot-wire probe was placed downstream the upper cylinder, Fig. 1 (b). So, the velocity fluctuations were gathered at such position at the turbulent wake of the cylinder. The velocity and pressure time-traces are displayed in Fig. 3 (a up to f), considering different p/d-ratios.

The u-velocity time-histories values on the upper cylinder are observed in Fig. 3 (a, b and c) for the three p/d-ratios to range from 2 m/s up to 18 m/s. Moreover, the signals stress some jumps that reveal the change in the wake topology (de Paula et al., 2012, 2013 and 2018, Neumeister et al., 2018).

On the other hand, the pressure time-traces on the upper cylinder are observed in Fig. 3 (d, e and f) for the three p/d-ratios but ranging between way smaller values between -450 and 60 Pa. The p/d-ratios showed great influence on pressure traces, as such for the lowest p/d (1.26) was observed to be negative due to the tight gap. The presented results show great similarity at the behavior of both pressure and velocity signals, responding the same way to flow phenomena. This agreement of behavior is corroborated by the findings of Neumeister (2015) and her following studies in Neumeister et al. (2018). Despite the same wake development from the pressure and velocity readings, the velocity time-traces showed to more sensitive to the changes, developing more intense fluctuations from the mean average.

According to de Paula et al. (2013), and Neumeister et al. (2018), the bistability phenomenon takes place whenever the wakes are near enough to interact with each other. This interaction yields two stable modes of wake topologies that randomly changes over time. Narrow and wide wakes are formed behind each cylinder, then last a time and then change

its topology afterwards. During such processes both instantaneous drag coefficient and vortex shedding are affected by the topology experienced by each cylinder (Summer, 2010, Alam et al., 2003, Vu et al., 2016 and Gomes et al., 2019). Based on such characterization the bistable flow is very well observed due to the jumps events in the velocity and pressure time-traces, Fig. 3 (a up to f). Note that any jump, in terms of velocity, lasts for some period of time (see Fig. 3 (b) from 5 s up to 8 s), it means that a new wake topology is formed. However, some differences can be seen as the gap, and therefore the p/d-ratio, between the cylinders increases. In Fig. 3 (b) shows the u-velocity for p/d-ratio 1.26. It is noteworthy that the number of jumps decreases as the p/d-ratio increases emphasizing that the wake interaction seems to fade away as the gap becomes wider. For the p/d-ratio equal to 3.00 is no longer possible, at least without using any mathematical tool, to visualize the changes in the wake's topology. Alam et al. (2003) and Roshko (1954) associated the different topologies, narrow and wide wakes, to high and low velocities behind the cylinders. By observing Fig. 3 (b), narrow and wide wakes are stably formed during the times 9 < t <11 s and 24 < t < 28 s, respectively.

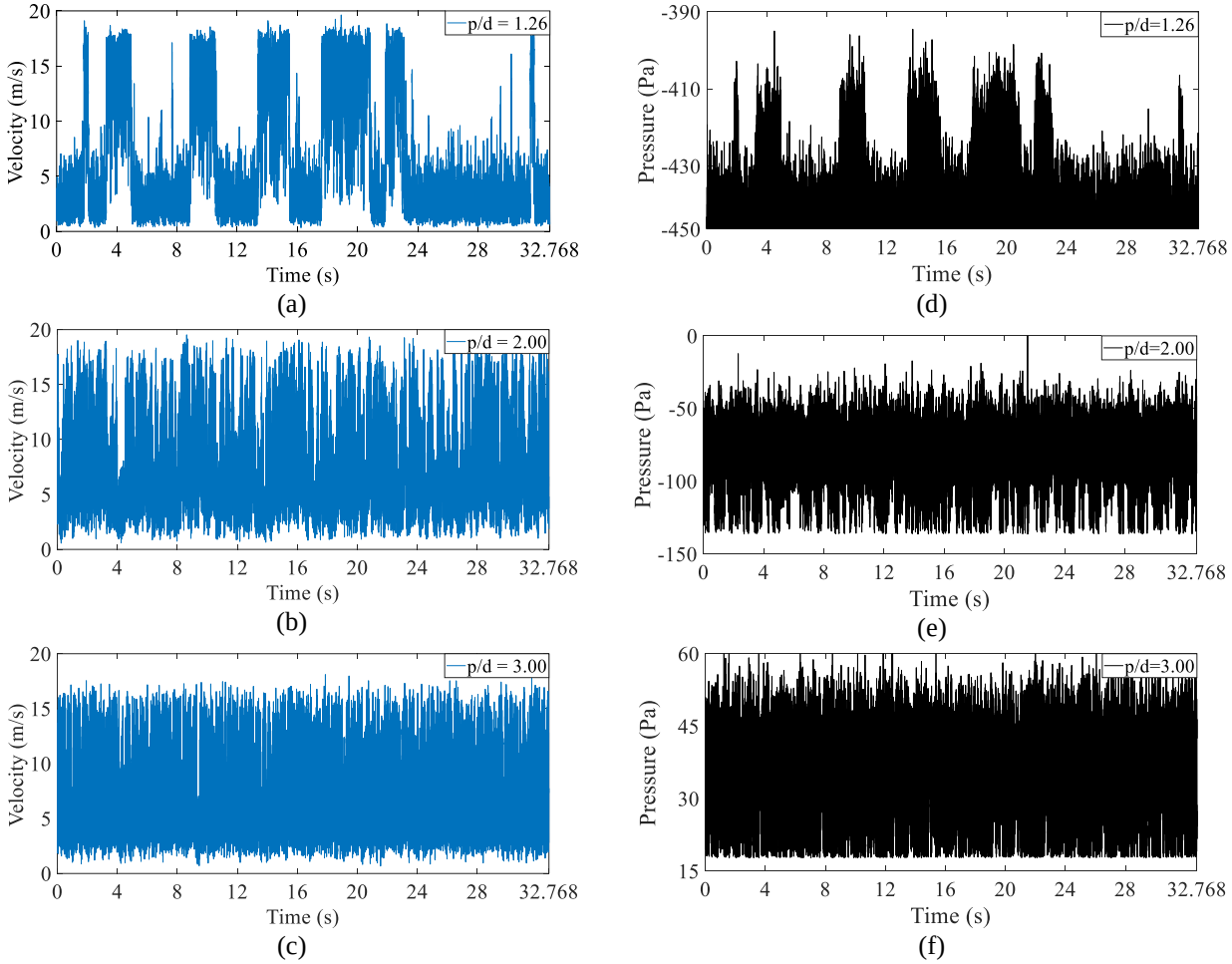

Figure 3. Instantaneous velocity fluctuations in the wakes. (a) p/d = 1.26; (b) p/d = 2.00; (c) p/d = 3.00; and instantaneous pressure fluctuations at the cylinder's surface at θ = 120º. (d) p/d = 1.26; (e) p/d = 2.00; (f) p/d = 3.00.

3.3 Wavelets Transform

The post-processing method of choice was the wavelets transform which was motivated by the fact that it allows us to represent a raw signal, unlike the Fourier transform, in terms of time and frequency simultaneously. The wavelet mathematical tool is composed by two subsignals: approximation (the average of adjacent elements, denoted by *a*) and details (difference of adjacent elements, denoted by *d*). The approximations represent the high-scale, low-frequency components of the signal, whereas, the details represent the low-scale, high-frequency components.

Both discrete wavelet transform (DWT) and continuous wavelet transform (CWT) can be used to approach flow phenomena. Melo et al. (2017) demonstrates that for a determined function, *f(t)*, considered to be a square-integrable function of a continuous time variable, *t*, the (CWT) is defined by Eq. (3):

$$W_{f(a,b)} = \int_{-\infty}^{\infty} f_{(t)} \psi_{a,b(t)} dt \tag{3}$$

, and the two-dimensional $\psi_{a,b(t)}$ is obtained from the mother-wavelet $\psi_{(t)}$ by simple scaling and translation, Eq. (4):

$$\psi_{a,b}(t) = \frac{1}{\sqrt{|a|}}\psi\left(\frac{t-b}{a}\right), \quad a,b \in R,\ \psi \in L^2(R) \tag{4}$$

, where the $a \neq 0$ and b denote the frequency and the time location, respectively, R is the set of real numbers, $L^2(R)$ is the square-summable time-series space of a specific $f(t)$. To avoid unnecessary calculus for every possible scale a and dilation b, the dyadic values are used for both scaling and dilation in (DWT) as displaced on Eq. (5):

$$a_j = 2^j,\ b_{j,k} = k2^j, \quad j,k \in Z \tag{5}$$

, where k and j represent the time and the frequency indices, respectively, and Z is the set of all integers. The wavelet expansion function is obtained in Eq. (6), through substituting Eq. (4) into Eq. (3), and may be rewritten as Eq. (7):

$$\psi_{j,k(t)} = 2^{-j/2}\psi(2^{-j}t - k), \quad j,k \in Z,\ \psi \in L^2(R) \tag{6}$$

$$W_f(j,k) = 2^{-j/2}\int_{-\infty}^{\infty} f(t)\psi(2^{-j}t - k)dt, \quad j,k \in Z,\ \psi \in L^2(R) \tag{7}$$

, which is the (DWT) of $f(t)$. A function f(t) also can be reconstructed by inverse of the (CWT) of Eq. (3) in the double-integral form or the (DWT) of Eq. (7) in the double-summation form. The (DWT) presented in Eq. (7) may be regarded as an attempt of preservation of the dominant features of the (CWT) of Eq. (3). Theoretically, the (DWT) can be justified as a judicious subsampling of (CWT) coefficients with dyadic scales. When compared with the discrete, the continuous wavelet transform can may obtain more accurate physical systems as it makes subtle information visible, although requiring more extensive computations for integrating over every possible scale, a, and dilation, b.

In Fig. 4 (a up to d) we present the results of pressure and velocity measured at the same instants and reconstructed via the (DWT) to clarify the wake interactions and the shifts between wakes. The wavelet type used was the Daubechies (Db20) with level 10. For this approach the wake was measured in terms of velocity downstream on the upper cylinder with a 0.9D far hot-wire probe, and a pressure transducer on the lower cylinder surface positioned at 150º. In order to produce this relation, the values of pressure and velocity were made dimensionless by dividing the point values by their mean value in each position. In Fig. 4 (a) we show the effectiveness of our function relating velocity and pressure. For this case only both probes were placed under the upper cylinder, in order to check the precision of our acquisition setup. With this analysis we can observe that the setup is successful on the determination of behavior of the wake, which suits our purpose of investigating the wake interactions and the bistable aspect by looking for the wake changes.

Fig. 4 (b), (c) and (d) exhibits the results of wake interactions obtained with both probes simultaneously in both cylinders (upper and lower). From these results we note the presence of wake topologies for every time-trace, as we notice the alternating topologies (WW and NW) on each cylinder (upper and lower), except for the transition instant (where signals cross). The results for the lowest p/d-ratio, 1.26, disposed on Fig. 4 (b), evidence clear shifts between wakes, as we can observe up to 7 shifts between narrow and wide wakes. The results for p/d = 1.26 also show the wakes changes between well defined velocity jumps from 0.5 m/s and 2.5 m/s, while for p/d = 2.00, Fig. 4 (c), and p/d = 3.00, Fig. 5 (d), the jumps occur between 0.8 m/s and 1.2 m/s, but not as uniform as the lowest spacing ratio. For the greater p/d-ratios, Fig. 4 (c) and (d), wake topology varies much faster, as it does not stablish uniform for a long period of time, as such one cannot quantify the number of changes by simply observing it as possible for the lowest p/d.

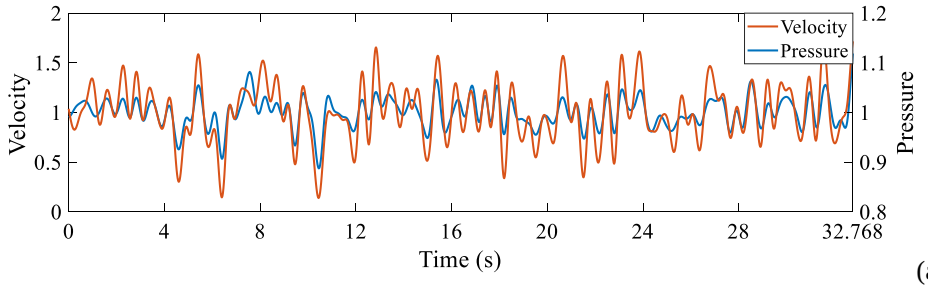

(a)

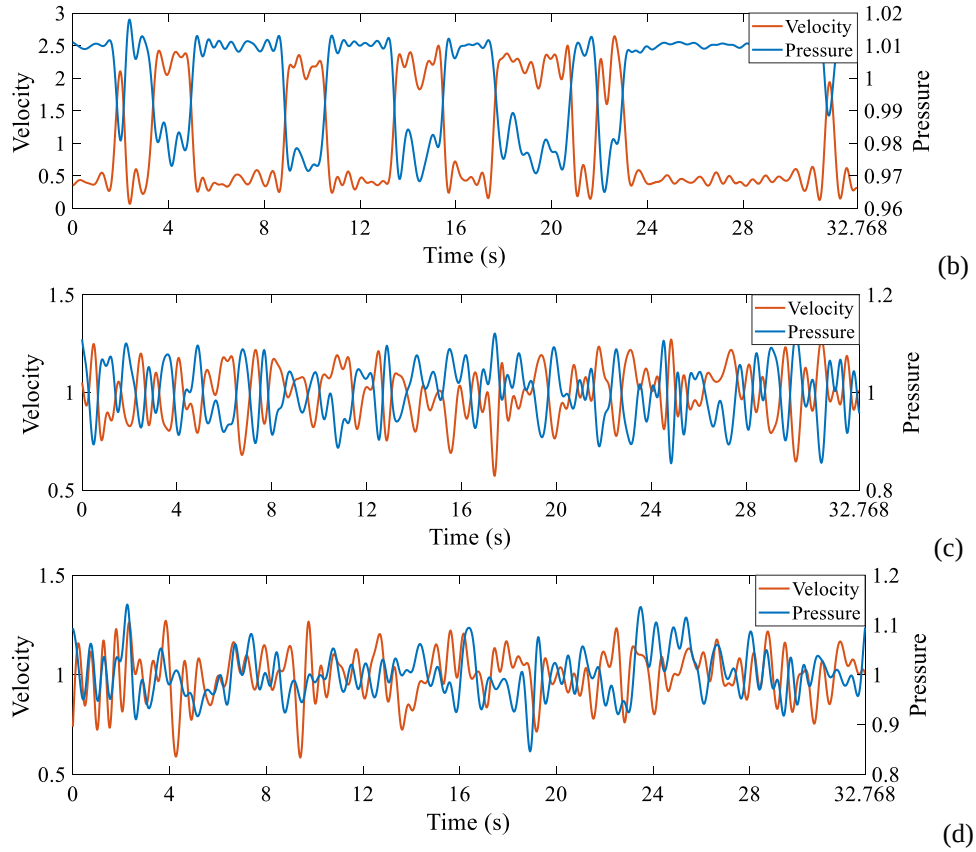

Figure 4. Fluctuations of velocity and pressure signals reconstructed with discreet wavelet transform. (a) validation; (b) p/d = 1.26; (c) p/d = 2.00; (d) p/d = 3.00.

Further, we aimed to investigate the time-traces through the continuous wavelet transform (CWT) package. Wavelet transformation is a set of coefficients that reconstructs a mother wavelet, providing good localization in both time and scale (frequency) domains via translations and dilatations. Continuous wavelet transform is used to approach the signals in the time-frequency domain. In Fig. 5 (a up to f) we show the results for the (CWT) reconstruction of pressure, on the surface of the cylinder at the position of 120°, and velocity readings, tangent downstream the cylinder, for the three p/d-ratios of study (1.26, 2.00 and 3.00). At first sight we note the similarity of behavior of the readings when compared to the raw signals analysis previously conducted. The p/d-ratio showed again great influence on the wake's energy levels, which is specially visible on the pressure results, Fig. 5 (d, e and f), whilst on the velocity results the same behaviors are noted but with lesser intensity. For the lowest p/d = 1.26 we can observe the wake shifts clearly, when again for the highest values a NW is present and for the lowest values a WW, but on the frequency scale. From this CWT approach we can observe the signals on the time-frequency domain, and then see that for this tight gap ratio the frequency is at most around at ~70 Hz, which further will be corroborated by the PSD analysis and the numbers of Strouhal found. For the p/d-ratios of 2.00 and 3.00 we note a frequency around 100 Hz, which also corroborates with the Strouhal findings. A remarkable observation is needed on the frequency results for the greatest p/d = 3.00, where the frequency is slightly different for the readings of velocity and pressure, both being apart 20 Hz from the mean 100 Hz.

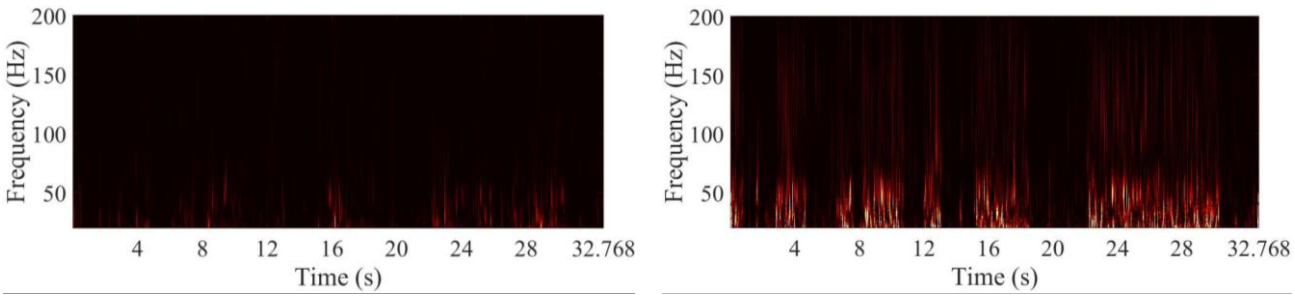

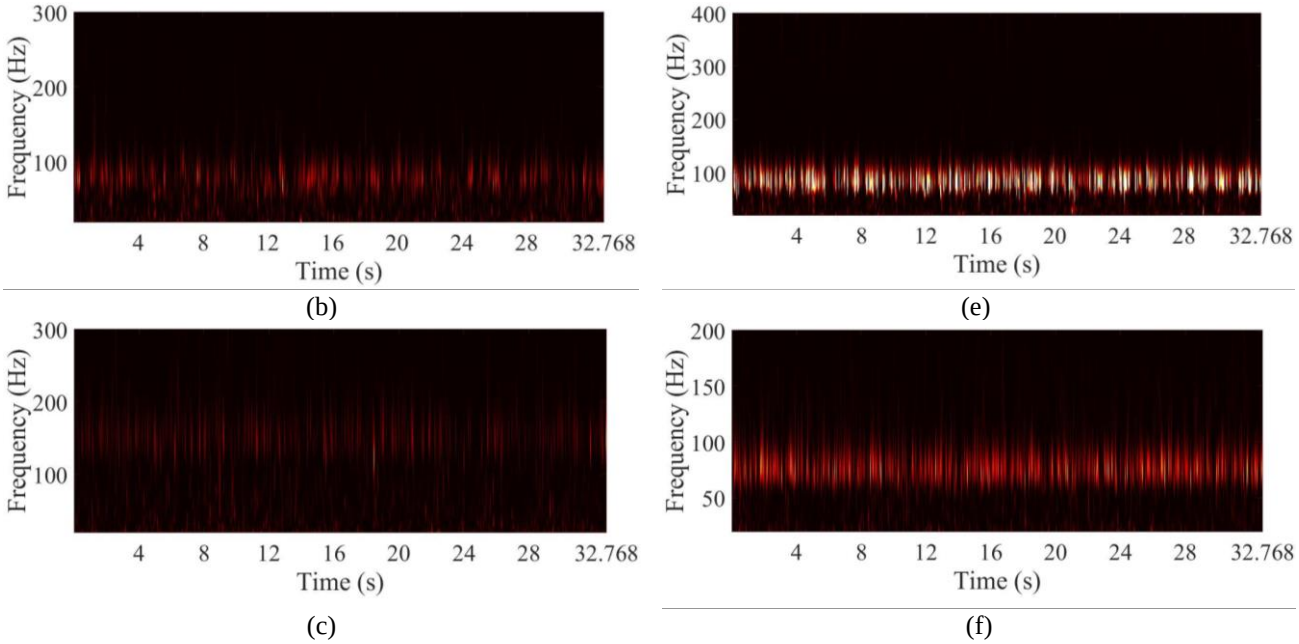

Figure 5. Continuous wavelet transform (CWT) of the velocity time-traces for (a) p/d = 1.26; (b) p/d = 2.00; (c) p/d = 3.00; and pressure time-traces for (d) p/d = 1.26; (e) p/d = 2.00; (f) p/d = 3.00.

We also investigated the velocity signals downstream the cylinder by means of the (CWT) package, applying Morlet wavelets, aiming the spectrograms of these instantaneous signals. This approach verifies the energy distribution of velocity fluctuations on the time-frequency domain. Figure 5 (a up to c) disposes the spectrogram of the velocity energy signals on the time-frequency domain. The results for the spacing ratio p/d = 1.26, Fig. 5 (a), where the shifts are well defined, low intensity energy peaks are observed on the first 8 seconds, what confers with the pure instantaneous velocity signals showed in Fig. 3 (a) and (b). These low values characterize the formation of a wide wake (WW). Therefore, a region with greater intensity energy peaks is also noticed, with frequencies distributed between 20 Hz and 100 Hz, which is related with the greater velocity values, characterizing a narrow wake (NW). The spectrogram presented for p/d = 2.00 in Fig. 5 (b) evidences the distribution of energy in a frequency band from 50 Hz to 90 Hz, with a more stable energy distribution on the time domain, when compared with the obtained with p/d = 1.26. The spectrogram of the p/d-ratio of 3.00, Fig. 5 (c), as the intermediate p/d-ratio evidences a uniform distribution of energy in a band of frequency stablished between 50 and 90 Hz. From this analysis we can observe that the intermediate p/d = 2.00 concentrates its energy on the frequency band of the p/d = 3.00, but the superior spacing ratio has far more concentrated and uniform peaks on 70 Hz, while the intermediate ratio is more well distributed on its range and presents low-energetic peaks outside the 50-90 Hz frequency band. We attribute this as a direct relation with the behavior of the velocity time-traces exposed previously as well as the number of wake shifts along the time.

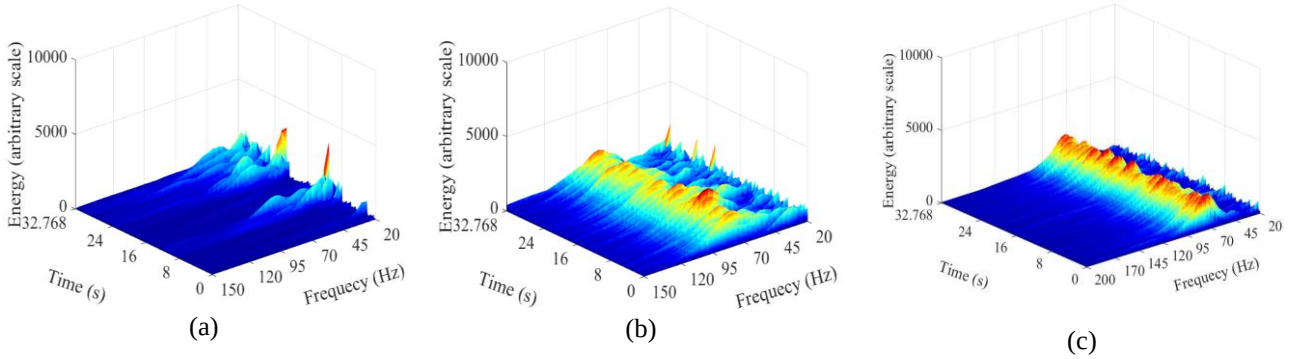

Figure 5. Energy spectrogram of the velocity signals. (a) p/d = 1.26; (b) p/d = 2.00; (c) p/d = 3.00.

3.4 Spectral Analysis

The dynamic analysis of the flow was also target of our investigation. Through power spectral density functions we look for quasi-periodic patterns in pressure and velocity time-traces. Fig. 6 (a up to g) show the power spectral density functions of the pressure time-traces for each cylinder and all p/d-ratios. Fig. 6 is made dimensionless in terms of Strouhal number on x-axis, whereas on the y-axis the power of the signal is made dimensionless through the density, the cylinder`s diameter and the free stream velocity, U_∞ (PSD). The dimensionless computations are stressed in Eq. (8):

$$St = \frac{f\,D}{U_\infty}; PSD = \frac{p^2}{\rho^2 U_\infty^3 D\,f} \tag{8}$$

, where *St* is the Strouhal number, *D* the cylinder`s diameter, ρ the density of the fluid and *p* the fluctuant part of the time-traces. In Fig. 6 (a) we show the spectral density function performed for a pressure time-traces in a single circular cylinder, under the same Reynolds number. The spectral densities are assigned to the angular position around the cylinder. The computations are made at the points near the angular position around the cylinder where the energy of the signal was found to be maximum, θ = 70°, 80° and 90°. From Fig. 6 (a) one can see that the setup is working in great agreement with the open literature. It is expected that under such Reynolds number the Strouhal must be about St ~0.21. Indeed, our outcomes have showed a very well highlighted dimensionless frequency of vortex shedding at St = 0.22. In our computations the frequency bandwidth was 3.90 Hz, making the Strouhal number ranging from 0.21 up to 0.23.

With the acquisition system approved we turn our attention to the cylinders arranged in pairs. Both cylinders presented the same fundamental frequency, nearby Strouhal 0.21. However, the Strouhal number seems to increase as the gap starts to appear. For the highest p/d-ratio, 3.00, the dimensionless frequency is quite close to that one found in a single cylinder. Fig. 6 (b) shows that the Strouhal number is very well marked at 0.23. For intermediated p/d-ratio, 2.00, the fundamental frequency slighted moves towards the higher values yielding St = 0.24 (Figure 6 (d)). On the other hand, the most intriguing result is the lowest p/d-ratio, 1.26, Fig. 6 (f). After computing the spectral density functions for all time-trace series of pressure fluctuations we could not identify any energetic peak in the spectrum. The proximity between the cylinders seems to suppress the vortex shedding. Nevertheless, for such p/d-ratio two low-energetic peaks appear at about St = 0.43 (whose appearance must be highlighted throughout the measurements). This low-energetic 0.43 peak was also found by Olinto (2005), whose identified a 0.42 Strouhal number for the p/d = 1.26. These peaks, due to their low energy, were not assigned (so far) to any fluid dynamic effect or bistable flow, since they also appeared in the single cylinder time-trace series spectral computations.

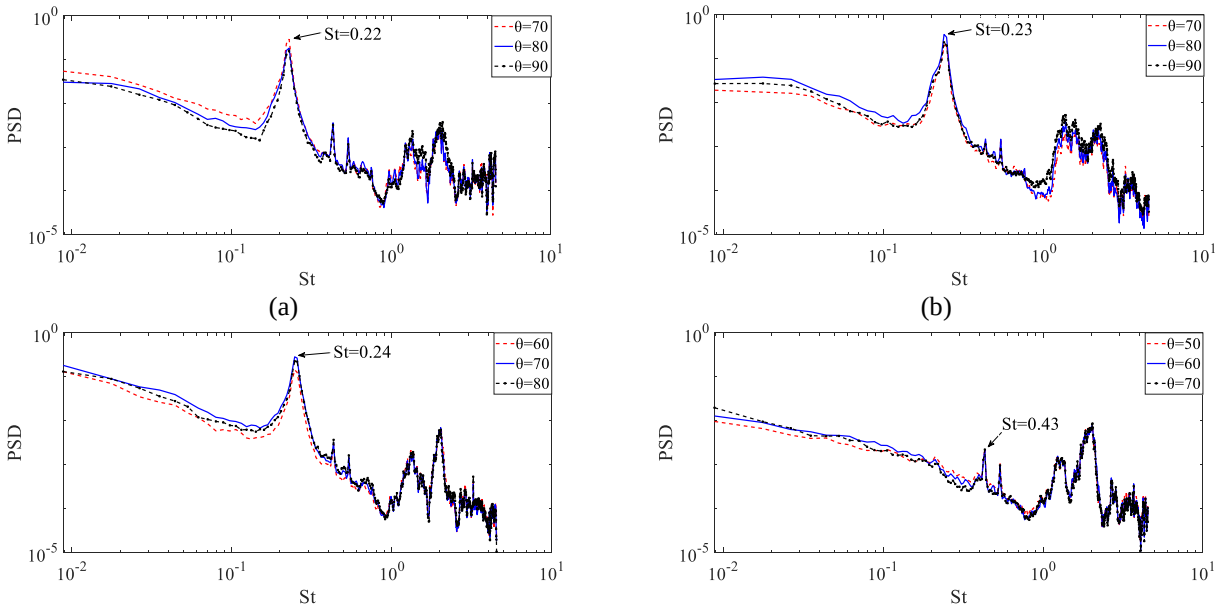

Figure 6. Power Spectral Density Function for pressure time-traces at different angular positions. (a) single cylinder; (b) p/d=3.00; (c) p/d=2.00; (d) p/d=1.26.

Further we also investigated the instantaneous velocity signals with the power spectral density analysis. Fig. 7 (a), (b) and (c) exhibits the energy peaks gathered from the measured velocity time-traces on the upper cylinder in terms of Strouhal. As for the pressure PSD approach, the Strouhal number on the x-axis is given by Eq. (8) as a function relating the fundamental frequency of the signal, while the power of the signal (PSD) is expressed on the y-axis and is made dimensionless through Eq. (8), which relates the fluid's density, the cylinder's diameter and the free stream velocity. The frequency bandwidth of the velocity computations was the same of the pressure's, 3.90 Hz, giving us a margin of error of 0.01. The spectral densities shown in figure 7 are assigned to the wake topologies (WW and NW) found during the velocity time-traces measurements. This approach is performed to investigate Strouhal number on both wake topologies, once the velocity values changes drastically along the wake topology changes, possibly causing an alteration on the Strouhal number. However, this was not seen, on all of the p/d-ratios the Strouhal numbers were found to be the same independent to the wake topology of measuring. The Strouhal was found nearby ~0.21, as did for the pressure signals, except for the lowest p/d, equal to 1.26, where a 0.14 was observed. Fig. 7 (b) and (c) both show a very well defined St of 0.22, p/d = 2.00, and 0.20, p/d = 3.00, respectively. As did for the pressure analysis, the most intriguing result is the lowest p/d-ratio, 1.26, Fig. 7 (a). The energy of this spacing ratio on both wake topologies was found very

low, so that we could not identify any energetic peak in the spectrum. The cylinders proximity seems to suppress the flow forces between them, causing a drastic reduction on the viscous forces hence vortex shedding and energy of the signals on the gap. The Strouhal found for these low-energetic peaks was 0.14. The same results were found by Olinto (2005), where the author found a St = 0.14 on the wide wake.

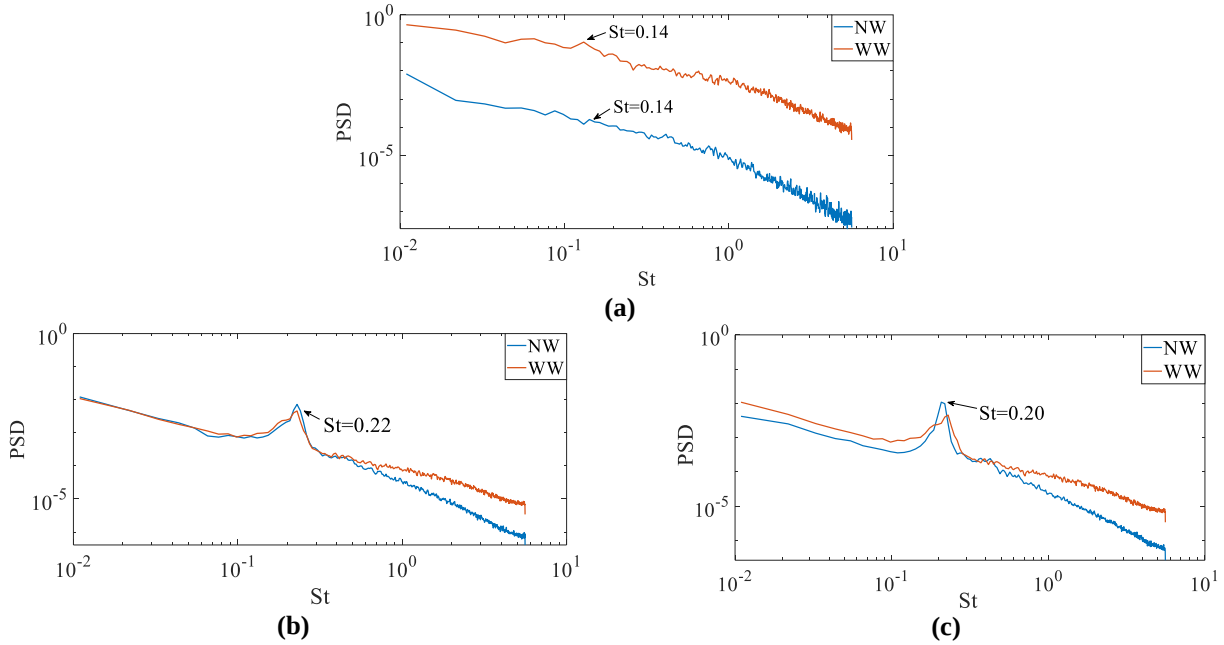

Figure 7. Power Spectral Density Function for velocity time-traces at both wide wake (WW) and narrow wake (NW) on the upper cylinder. (a) p/d = 1.26; (b) p/d = 2.00; (c) p/d = 3.00.

4. CONCLUSIONS

This work is aimed to study the characteristics of the turbulent flow over two side-by side circular cylinders. The tubes were disposed apart to each other by a distance, between their centers, named P. An experimental campaign was carried out in order to measure the pressure fluctuations, around the cylinders, and the velocity fields, downstream the cylinders, for three p/d-ratios equal to 1.26, 2.00 and 3.00, under the same Reynolds number, Re = 1.78×10^4. The second target of our work was to implement image processing and spectral density analysis techniques to investigate the behavior of the measurements over the time-frequency domain.

Our acquisition apparatus was first validated by the readings of boundary layer detachment and vortex shedding on a single cylinder, as we found it to occur at ~80º. It was also corroborated by the PSD approach identifying a St ~0.21.

As regards to the mean pressure for different p/d-ratios the outcomes have shown that the proximity of the tubes plays an important role in the pressure distribution. The stagnation and boundary layer detachment points are were found to move towards the tight gaps as p/d-ratio decreased.

The spectral analysis for the pressure time-traces showed fundamental frequencies associated to vortex shedding in both tubes. The Strouhal numbers were found slightly higher than we found in a single cylinder, for p/d-ratio 2.00 and 3.00. However, for the lowest p/d-ratio (1.26) our results on spectral analysis were not conclusive, as no energetic peaks were found for such p/d-ratio.

The velocity time-traces showed again the great influence the p/d develops under the wake topologies past the cylinders. The raw time-traces show an evident pattern of wake shifts for the lowest p/d = 1.26, but not for the others as expected. From the wake interactions measured simultaneously at both cylinders in terms of pressure and velocity we observed a tendency of changes on the intermediate p/d = 2.00 but not full shifts as easily seen for p/d = 1.26, while the greatest ratio behaved as a single cylinder.

Spectral density analysis technique of the velocity readings us to note the similarity between the Strouhal numbers found from two different readings. Apart from the observations with p/d = 1.26 which corresponded to ~0.14. This value is also due to low energetic signals gathered due the tight gap between the cylinders which tends to inhibit the viscous forces. Later, these low energetic peaks were found to be in agreement with Olinto (2005) findings, which lead us to identify a correlation between the wake topology and the St number (0.14 while on a WW and 0.43 on a NW).

A bistable flow behavior was observed for the lowest p/d through the wavelet transform technicque. Both (DWT) and (CWT) transforms made possible to identify a intermittent and random pattern flow, these being the characteristics of a bistable flow. Whilst for the other spacing ratios bistability was not found. For p/d = 3.00 was expected to behave as a single cylinder, as it did, while for p/d = 2.00 which is on the edge of the bistable appearance range defined by Alam et al. (2003) (1.2 < p/d < 2.0), a tendency to shift wakes was observed but not developed and uniform changes which we can not understand as an intermittent pattern hence bistable.

5. ACKNOWLEDGEMENTS

The first and second authors thank to Centro Universitário do Distrito Federal – UDF for the support incentive given for the execution of this research. The authors also thank to FAP-DF (n° 0193.001356/2016) for supporting them with a fellowship during this research. Jhon Goulart thanks to FAP- DF for supporting him in order to purchase the hot-wire anemometry system through the project n° 193.001.158/2015 and to National Council for Scientific and Technological Development – CnPq, for supporting the research on the subject through the process n° 408869/2016-0.

6. REFERENCES

Afgan, I., Kahil, Y., Benhamadouche, S., Sagautm P., 2011. "Large eddy simulation of the flow around single and two side-by-side cylinders at subcritical reynolds numbers". *Journal of Physics of Fluids*, 23(7), pp. 075101-1.

Ahmad, N., Bihs, H., Myrhaug, D., Kamath, A., Arntsen, O.A, 2018. "Three-dimensional numerical modelling of wave-induced scour around piles in a side-by-side arrangement". Coastal Engineering, pp. 132-151.

Alam, M. M., Moriya, M., Sakamoto, H., 2003. "Aerodynamics characteristics of two side-by-side circular cylinders and application of wavelet analysis on the switching phenomenon". *Journal of Fluid and Structures*, pp. 325-346.

Alam, M. M., Zheng, Q.,Hourigna, K., 2017. "The wake and thrust by four side-by-side cylinders at a low Re". Journal of Fluids and Structures, 70 (2017), pp. 131–144.

de Paula, A. V., Endres, L. A. M., Möller, S. V., 2012. "Bistable features of the turbulent fow in tube banks of triangular arrangement". *Nuclear Engineering Design* 249:379–387.

de Paula, A. V., Möller, S. V., 2013. "Finite mixture model applied in the analysis of a turbulent bistable flow on two parallel circular cylinders''. *Nuclear Engineering and Design*, *264*, 203-213.

de Paula A. V., Möller S. V., 2018. "On the chaotic nature of bistable fows". *Exp Therm Fluid Science* 94:172–191.

Giacomello, M. V., Rocha, L. A. O., & Silvestrini, J. H., 2006. "Simulação Numérica De Escoamentos Ao Redor De Cilindros Com Transferência De Calor". *5a Escola de primavera de transiçao e turbulência, Rio de Janeiro, Brasil*.

Gomes, T. F., Sandoval, D. C., Goulart, J. N., 2019. "Numerical sutdy of turbulent flow over circular cylinders side-by-side under diffferent reynolds numbers". *Revista Interdisciplinar de Pesquisa em Engenharia*, vol.5 (2).

Goulart, J. N. V., Olinto, C. R., Moler, S. V., 2003. "Experimental analysis of the turbulent flow inside a tube bank with baffle plates". *17th International Congress of Mechanical Engineering, São Paulo, Brasil.*

Kang, S., 2003. "Characteristics of flow over two circular cylinders in a side-by-side arrangement at low Reynolds numbers". *Journal of Physics of Fluids*, *15*(9), 2486-2498.

Kim, S., Alam, M.M, 2015. "Characteristics and suppression of flow-induced vibrations of two side-by-side circular cylinders". Journal of Fluids and Structures, pp. 629-642.

Melo, T., Goulart, J. N. V., Anflor, C. T. M., Santos, E., 2017. "Experimental investigation of the velocity time-traces of the turbulent flow in a rectangular channel with a lateral slot". *European Journal of Mech Fluids*, pp. 130-138.

Moffat, R. J., 1988. "Describing the Uncertainties in Experimental Results". *Expr Thermal and Fluid Sci*, v. 1, pp. 3-17.

Neumeister, R. F., Petry, A. P., Moller, S. V., 2018. "Characteristics of the wake formation and force distribution of the bistable flow on two cylinders side-by-side". *Journal of the Brazilian Society of Mech Sci and Eng*, pp. 40-564.

Olinto, C. R., 2005. "Estudo experimental das características do escoamento turbulento nas primeiras fileiras de bancos de tubos". Msc. Thesis, Universidade Federal do Rio Grande do Sul, Porto Alegre, Brasil.

Olinto, C. R., Indrusiak, M. L. S. and Möller, S. V., 2006. "Experimental study of the bistable flow in tube arrays". *Journal of the Brazilian Society of Mechanical Sciences and Engineering*, Vol. XXVIII, No. 2, pp. 233-241.

Olinto, C. R., Endres, L. A. M. and Möller, S. V., 2009. "Experimental study of the characteristics of the flow in the first rows of tube banks". *Nuclear Engineering and Design*, Vol. 239, pp. 2022-2034.

Pang, J. H., Zong, Z., Zou, L., Wang, Z., 2016. "Numerical simulation of thr flow around two side-by-side circular cylinders by IVCBC vortex method". *Ocean Engineering*, 119, pp. 86-100.

Roshko, A, 1954. "On the development of turbulent wakes form vortex streets". National Advisory Comitte for Aeronautics (NACA) Technical Report, pp. 1191.

Sumner, D., 2010. "Two circular cylinders in cross-flow: a review". *Journal of Fluids and Structures*, *26*(6), 849-899.

Vu, H. C., Ahn, J., Hwang, J. H., 2016. "Numerical simulation of flow past two circular cylinders in tandem and side-by- side". *KSCE Journal of Civil Engineering*, pp. 1597-1604.

Wang, Z. J., & Zhou, Y., 2005. "Vortex interactions in a two side-by-side cylinder near-wake". *International journal of heat and fluid flow*, *26*(3), 362-377.

Zukauskas, A., 1972. "Heat transfer from tubes in crossflow". *Advances in heat transfer v*ol. 8, pp. 93-160.

Zukauskas, A., Katinas, V. J., Perednis, E. E., & Sobolev, V. A., 1980. "Viscous flow over inclined in-line tube bundles, and vibrations induced in the latter". *Fluid Mechanics-Soviet Research*, *9*(4).

Zukauskas, A., Katinas, V., 1988. "Fluid dynamic forces on vibrating tubes of heat exchangers in cross-flow". *Journal of Fluids and Structures*, *5*(3), 279-298.

7. RESPONSIBILITY NOTICE

The authors are the only responsible for the printed material included in this paper.